POLITECNICO DI TORINO
Repository ISTITUZIONALE

Potential of ammonia as hydrogen storage for future electrified aircraft

(Article begins on next page)

29 December 2025

Potential of ammonia as hydrogen storage for future electrified aircraft

Maria Chiara Massaro [a] , Federico Aluia [a], Roberta Biga [b], Grazia Accardo [b],
Alessandro Hugo Antonio Monteverde [a],*

[a] *Department of Applied Science and Technology, Politecnico di Torino, Corso Duca degli Abruzzi 24, 10129 Torino, Italy*
[b] *Leonardo. Innovation Labs & Intellectual Property, Corso Francia 426, 10146 Torino, Italy*

ABSTRACT

The implementation of hydrogen as a clean aviation energy vector faces challenges in onboard storage and transportation due to its low volumetric energy density and the strict weight and space constraints of aircraft. This study introduces a breakthrough approach, leveraging liquid ammonia as a hydrogen carrier for electrified aircraft propulsion, an area largely unexplored compared to land and maritime applications. Ammonia's high hydrogen content, ease of storage, and existing infrastructure make it a compelling alternative to conventional hydrogen storage methods.

An integrated system design is presented, combining ammonia storage, a high-efficiency cracking reactor for on-demand hydrogen release, and a purification unit ensuring compatibility with the conversion system, which consists of proton exchange membrane fuel cells (PEMFCs) and their associated balance-of-plant components. To optimize performance and reduce the overall system footprint, a thermal integration strategy is implemented.

The paper provides a quantitative assessment of the system's feasibility in a regional aircraft, demonstrating a gravimetric hydrogen storage index of 9.1%, rivaling state-of-the-art physical storage solutions, and identifying key technological gaps that must be overcome to enhance system performance and competitiveness with conventional kerosene-based propulsion.

By addressing the specific challenges of hydrogen storage in aviation, this work provides new insights into the potential of ammonia-based systems and their role in advancing sustainable airborne propulsion technologies.

1. Introduction

Aviation accounts for approximately 13.9 % of CO_2 transport-related emissions and 5 % of global greenhouse gas emissions [1]. With global aviation demand expected to increase by 4.5 % annually [2], the aviation sector must implement substantial and disruptive strategies to effectively address its environmental footprint. These strategies include developing highly innovative technologies, electrifying part of the fleet, and significantly scaling up sustainable aviation fuels (SAFs) [3].

Hydrogen-based propulsion systems represent the most effective solution for aircraft up to the short-range category, providing a substantial reduction in emissions compared to conventional propulsion systems [3].

To successfully implement hydrogen-based mobility, hydrogen must be stored safely, with technical advancement, economic viability, and environmental friendliness. The most established methods, such as liquid and compressed hydrogen, offer simplicity and rapid release but

require significant space and present operational risks, making them challenging for applications like in-flight use [4].

An alternative approach could involve the use of liquid fuels, which chemically store hydrogen, enabling easy transportation and long-term storage [5]. Ammonia (NH_3) is a promising candidate due to its ability to be liquefied under mild conditions and stored in a simple, inexpensive pressure vessel. Ammonia is a carbon-free fuel, with a high hydrogen content by weight (17.65 wt%), offering a volumetric hydrogen density 45 % higher than liquid hydrogen [6]. In addition, the infrastructure for storing and transporting ammonia is well established as a result of its widespread use in fertilizer production [7].

Table 1 compares ammonia's performance metrics with other energy storage technologies in terms of energy density, production and conversion efficiencies, CO_2 emissions, transmission and storage costs, and safety issues.

In an energy system, ammonia can be used directly as liquid fuel, or indirectly as hydrogen chemical storage medium [9]. As a liquid fuel, ammonia can be fed in internal combustion engines (ICEs) or fuel cells

---

Nomenclature

Symbols

A_{HF}	Area of the single hollow fiber, m^2
$A_{HF,eff}$	Effective area of hollow fibers, m^2
$A_{packing}$	Area of square packing into membrane reactor, m^2
c_p	Specific heat capacity, kJ kg^{-1} K^{-1}
$c_{p,coolant}$	Specific heat capacity of coolant, kJ kg^{-1} K^{-1}
D_{ad}	Diameter of adsorption column, m
D_i	Internal diameter, mm
$D_{packing}$	Hollow fiber diameter, m
D_{pore}	Pore diameter for hollow fiber, m
e	Thickness, mm
E_{cell}	Operative fuel cell potential, V
E_{th}	Thermodynamic fuel cell potential, V
f	Function for determination of tank thickness
F	Faraday constant, C mol^{-1}
h	Altitude, m
k	kinetic constant, s^{-1}
i	Fuel cell current, A
L_{ad}	Length of adsorption column, m
L_{HF}	Length of the hollow fiber, m
$\dot{m}$	Mass flow rate, kg s^{-1}
$\dot{m}_{coolant}$	Mass flow rate of coolant, kg s^{-1}
M_{air}	Molecular weight of air, g mol^{-1}
M_{H_2}	Molecular weight of hydrogen, g mol^{-1}
M_{NH_3}	Molecular weight of ammonia, g mol^{-1}
mol_{NH_3}	Mol of ammonia to remove from the produced hydrogen, mol
N_{cell}	Number of cells in fuel cell stack
N_{HF}	Total number of hollow fibers
$N_{HF,baseline}$	Total number of hollow fibers in the baseline application
N_{stack}	Number of fuel cell stacks
p	Operative pressure, MPa
Q_{HTC}	Heat to be removed from fuel cell (in the high thermal cooling system), kW
Q_{LTC}	Heat to be removed in the low thermal cooling system, kW
R_m	Tensile strength, MPa
$R_{p,0.2}$	Yield strength, MPa
T_{ad}	Operative temperature of adsorption column, °C
$t_{coolant}$	Circulation time of liquid coolant into the circuit, s
$T_{in,air}$	Air temperature at radiator inlet, °C
$T_{in,coolant}$	Coolant temperature at fuel cell inlet, °C
$T_{in,compr}$	Temperature at compressor inlet, °C
$T_{in,LTC}$	Coolant temperature at LTC system inlet, °C
$T_{in,air}$	Air temperature at radiator outlet, °C
$T_{out,coolant}$	Coolant temperature at fuel cell outlet, °C
$T_{out,LTC}$	Coolant temperature at LTC system outlet, °C

$V_{eff,HFR}$	Effective volume of hollow fiber reactor, m^3
$\dot{V}_{NH_3}$	Volumetric flow rate of ammonia, m^3 s^{-1}
V_r	Reactor volume, m^3
U	Global heat coefficient, kJ kg^{-1} K^{-1}
w_{ad}	Adsorption capacity, mmol$_{NH3}$ g$_{AC}^{-1}$
$W_{AC,eff}$	Effective mass of activated carbon, kg
W_{ad}	Total mass of adsorption column, kg
W_{cat}	Mass of catalyst, kg
$W_{emptycolumn}$	Mass of empty adsorption column, kg
W_{HFR}	Weight of hollow fiber reactor, kg
y_{O_2}	Volumetric concentration of oxygen in air
x_{NH_3}	Conversion of ammonia
β	Compression ratio
γ	Polytropic exponent
ΔH_r	Enthalpy of reaction, kJ mol^{-1}
ε	Heat exchange effectiveness
ε_{HF}	Porosity of the hollow fiber substrate
η_{is}	Isentropic efficiency
η_{em}	Electro-mechanic efficiency
λ_{air}	Air stoichiometry for fuel cell reaction
λ_{H_2}	Hydrogen stoichiometry for fuel cell reaction
ρ	Density, kg m^{-3}
ρ_{AC}	Density of activated carbon, kg m^{-3}
$\rho_{Al_2O_3}$	Density of the hollow fiber material, kg m^{-3}
ρ_b	Density of reactor bed, kg m^{-3}
τ	Residence time, s

Abbreviations

AC	Activated carbon
DAFC	Direct ammonia fuel cell
DSU	Dissociation and separation unit
FC	Fuel cell
GT	Gas turbine
HF	Hollow fiber
HFR	Hollow fiber reactor
HGS	Hydrogen Generation System
HTC	High thermal cooling
HT-PEMFC	High-temperature proton exchange membrane fuel cell
ICE	Internal combustion engine
LHV	Low heating value, MJ kg^{-1}
LTC	Low thermal cooling
MTOW	Maximum take-off weight
OEW	Operational empty weight
PEMFC	Proton exchange membrane fuel cell
SAF	Sustainable aviation fuel
SOFC	Solid oxide fuel cell
T	Temperature
TMS	Thermal management system

such as solid-oxide fuel cells (SOFCs), high-temperature proton exchange membrane fuel cells (HT-PEMFCs) or direct ammonia fuel cells (DAFCs). However, the direct use of ammonia is limited by high ignition energy, slow flame propagation, and NO$_x$ emissions, while fuel cells struggle with slow dynamics at high operating temperatures or low energy efficiency for the DAFCs [9,10].

A more practical approach for mobile applications involves the indirect use of ammonia, which can be stored on-board and converted into hydrogen for feeding the energy system [9,10]. In the latter case, the hydrogen, chemically bound within the ammonia molecule, is released through a catalytic decomposition process.

The hydrogen release process occurs via ammonia decomposition (cracking), which follows the endothermic reaction [11]:

$$2NH_3 \rightarrow N_2 + 3H_2 \qquad \Delta H_r = 46.2 \ kJmol^{-1} \qquad (1)$$

The cracking reaction is endothermic, thermodynamically favored by low pressures and high temperatures [11]. It is facilitated by catalysts such as nickel, ruthenium, or cobalt-based materials to enhance efficiency and reduce energy consumption [12]. The released hydrogen can then be directly fed into a fuel cell or combustion system for propulsion.

The conversion and reconversion processes result in an energy loss of 7 % to 18 %, depending on system size and location [13]. While small-scale, high-temperature cracking is commercially available, more efficient lower-temperature methods are needed to improve efficiency, cost, purity, and scalability—key concerns for applications like fuel cell vehicles, which require ammonia concentrations below 0.1 ppmv [4,7].

The use of membrane reactors enhances yields by integrating hydrogen production and separation in a single unit [14-16]. Another approach for reactor optimization involves the use of an autothermal unit, which enables a continuous, self-sustained hydrogen supply in a compact structure through alternating reductive and oxidative zones, using the combustion of part of ammonia to drive the endothermic decomposition reaction [17,18].

This paper shifts its focus from ammonia conversion reactor technology to a more comprehensive view of ammonia storage technology. Many studies in the literature are exploring the use of ammonia for on-board energy storage in transportation.

Stolz et al. [7] demonstrated the potentialities of ammonia as a storage solution for powering Europe's bulk cargo shipping through a comprehensive evaluation of various fuels and energy converters. They compared hydrogen, ammonia, methane and diesel as fuels, and assessed different energy converters, like electric motors, ICEs, SOFCs and PEMFCs. After considering factors such as gravimetric energy density constraints, electricity demand for fuel production, and overall costs, they found ammonia to be a well-balanced carbon-free fuel option [7].

To use ammonia on-board as a fuel with minimal modifications to the propulsion system, Comotti et Frigo [19] designed a system where ammonia is directly fed into conventional ICEs with a combustion promoter. Ammonia is stored on-board and converted into hydrogen within the thermally integrated Hydrogen Generation System (HGS) for efficient fuel utilization [19].

To enhance thermal integration and efficiency, many studies have explored the potential use of ammonia storage in hybrid systems featuring both ICE and fuel cells. Ezzat at Dincer [20] proposed two integrated vehicular systems utilizing ammonia as source. The first system is powered by an ICE, while the second is a hybrid configuration with a PEMFC as the main power source and an ICE providing additional power. Both systems utilize a mixture of ammonia and hydrogen generated on-board from ammonia in a thermally integrated dissociation and separation unit (DSU). Integrating the fuel cell with the ICE improved overall efficiency, despite potential increased costs [20]. Al-Hamed et Dincer [21] instead, designed a system combining a SOFC-gas turbine (SOFC-GT) with an ammonia DSU and a PEMFC for on-board hydrogen production and utilization in a passenger locomotive. Waste heat from the ammonia-SOFC was used to produce hydrogen in the DSU for PEMFC. The system showed an efficiency of 61.2 %, highlighting the advantages of waste heat recovery [20].

Other researchers focused on the use of ammonia in full-electric solutions, with fuel cells as converters. For example, Di Legge et al. [22] investigated the direct use of ammonia in SOFCs in a feasibility study for a 130 kW general aviation case study. They introduced a semi-

empirical model showing the effectiveness and potential of ammonia-powered fuel cell technology for aircraft propulsion. The analysis indicated a 5.9 % reduction in fuel consumption during a one-hour mission compared to kerosene-fueled aircraft, highlighting the advantages of using ammonia as a fuel source [22]. On the other hand, Cha et al. [18] combined ammonia with PEMFCs to create a 1 kW hydrogen power pack, generating high-purity hydrogen via a catalytic reactor and a zeolite adsorption tower. Surplus hydrogen from the fuel cell was used to supply the required heat for ammonia cracking, boosting the system's overall efficiency to above 49 % while eliminating the need for an external heat source. Applied to a drone, the system enabled over 4 h of flight, significantly longer than the 14-minute flight time achieved with a lithium-polymer battery [18]. Similarly, Ye et al. [23] designed electric propulsion systems for two different scales of maritime applications (i.e., water taxi and container ship), using ammonia with an integrated cracking system. The study examined three storage options: liquid and compressed hydrogen, and ammonia with an integrated cracking system. All storage methods met ship volume and mass constraints except for gaseous hydrogen, which was found to be impractical for cargo ships. Electrified systems, using green hydrogen and ammonia, achieved nearly zero operational emissions, leading to a 90 % reduction in life-cycle GHG emissions, despite higher costs compared to the current fuel–oil engine setups [23]. Moreover, Lin et al. [24] developed a physical–chemical model of an indirect ammonia PEMFC system with integrated catalytic reactor for ammonia decomposition, investigating different layouts to optimize energy efficiency and economic viability. Hunter et al. [25] showcased a compact experimental setup using ammonia to produce 40 W of electricity in a heat and mass balanced system. The system included a catalytic reactor with light metal amide-imides, a post-reactor gas purification column and a 100 W PEMFC. They also suggested HT-PEMFCs as an intermediate solution between SOFCs and PEMFCs, offering better thermal integration and greater tolerance to feed impurities, potentially eliminating the need for purification [25]. On the other hand, Cinti et al. [26] proposed a design for a heat-integrated ammonia-fuelled HT-PEMFC system that included a cracking reactor and heat exchangers. Experimental tests on a short-stack HT-PEMFC fuelled with nitrogen and hydrogen showed a total efficiency of 40 % at a power density of 0.21 W cm^{-2} [26].

Previous studies have primarily focused on land and maritime applications, leaving the use of ammonia as a hydrogen carrier for aviation largely unexplored. Moreover, the stringent weight and volume constraints in aviation make hydrogen storage a critical challenge, limiting current solutions to small-scale or hybrid configurations [4].

This study presents a systemic evaluation of ammonia-based hydrogen storage for an all-electric propulsion system in megawatt-class regional aircraft, utilizing onboard hydrogen generation via

Table 1
Comparison of performance metrics for batteries, hydrogen, and ammonia.

	Li-ion battery	H$_2$ 1 bar, 25 °C	Compr. H$_2$ 700 bar, 25 °C	Liquid H$_2$	Liquid NH$_3$
Grav. density kWh kg^{-1} [7]	0.17	33.3	1.40	2.50	3.60
Vol. density MWh m^{-3} [7]	0.30	0.003	0.60	1.32	2.70
Well-to-tank[a] efficiency [7]	0.95	0.70	0.60	0.55	0.54
Tank-to-wake[a] efficiency [7]	1	0.60 (PEMFC)	0.60 (PEMFC)	0.60 (PEMFC)	0.80x0.60 (cracking + PEMFC)
Well-to-wake efficiency	0.95	0.42	0.36	0.33	0.26
CO$_2$ emissions[b] g kWh^{-1} [8]	Not available	0 – 114 (electrolysis)	0 – 114 (electrolysis)	0 – 114 (electrolysis)	0 – 178 (electrolysis + Haber-Bosch)
Transmission costs $ kWh^{-1} [8]	/	Not applicable	0.060	>0.060[c]	0.004
Storage costs $ kWh^{-1} [8]	/	Not applicable	0.030	>0.030[c]	0.007
Safety issues [4]	/	Not applicable	High-pressure tank	Cryogenic tank, boil-off	Toxicity, corrosion

[a] *Well-to-tank efficiency refers to the production of fuel in its storage form, while tank-to-wake efficiency refers to fuel conversion into electricity.*
[b] *derived from fuel production, with a range depending on the proportion of renewable energy used during electrolysis.*
[c] *Due to the lack of data on transmission and storage costs for liquid hydrogen, values are assumed to be higher compared to compressed hydrogen.*

ammonia cracking to supply PEMFCs. The proposed system integrates ammonia storage, a high-efficiency cracking reactor, and a purification unit to ensure fuel cell compatibility, with a thermal integration strategy to enhance performance and reduce system footprint.

Beyond feasibility assessment, this work quantifies the impact of ammonia storage on aircraft payload relative to conventional kerosene propulsion, demonstrating its potential as a competitive hydrogen storage solution with advantages in onboard safety and cost-effective hydrogen transport. By identifying key technological challenges and optimization pathways, this study establishes the groundwork for ammonia-based hydrogen storage in sustainable, electrified aviation.

2. Methodology

2.1. System and case study description

The hydrogen storage system for an aircraft with fuel cell propulsion includes all equipment that facilitates the supply of hydrogen to the fuel cell, meeting the required temperature, pressure, and purity conditions starting from ammonia.

The sizing process involved identifying system components and selecting their types. As reported in Fig. 1, key components of the storage system include:

- the tank, which stores ammonia in liquid form at 25 °C and 10 bar;
- a heating section to achieve the required fluid temperature at the reactor's inlet;
- a reactor facilitating the cracking reaction;
- a hydrogen purification section to remove nitrogen and traces of ammonia harmful to the fuel cell system;
- Compression and cooling sections to bring the purified hydrogen to nominal conditions at the fuel cell system's inlet.

To establish the definitive architecture of the storage system, a thermal optimization study was conducted to achieve optimal integration between the storage and fuel cell systems.

Finally, the fuel cell system was sized, including the stacks and the balance of plant.

The sizing of all components was performed using a regional aircraft as a case study. In particular, a retrofitting of the ATR72-600 was undertaken, involving the replacement of the conventional kerosene propulsion system with a properly sized electrified system. This electrified system encompasses the storage section, the fuel cell system, and an electric motor responsible for converting the electrical power generated by the fuel cell system into mechanical power.

Once established the power requirement for the reference commercial aircraft, an iterative procedure was executed to determine the hydrogen necessary for the fuel cell to meet the on-board power demands, including both propulsion and auxiliary equipment needs. The determined quantity of hydrogen for the fuel cell was then used to calculate the corresponding amount of ammonia, enabling the sizing of all components and the thermal integration of the entire system with an optimization perspective.

Table 2 reports the main features of ATR72-600 and the components' weight for the kerosene-based propulsion system.

Table 2
ATR72-600 features.

Technical characteristics	Value	Unit
Number of passengers	72	
Take-off power (half-wing)	1845.6	kW
Max. cruise power (half-wing)	1589.8	kW
Maximum altitude	25,000	Ft
Maximum payload	7550	kg
Maximum take-off weight (MTOW)	22,800	kg
Operational empty weight (OEW)	13,450	kg
Kerosene-based system		
Structure	10,478	kg
Fuel	1800	kg
Fuel system	1667	kg
Thermal engine	481.7	kg

2.2. Hydrogen storage section

2.2.1. Storage tank section

Ammonia was supposed to be stored in a pressurized vessel at ambient temperature and 10 bar.

The procedure carried out to determine the volume of the storage tank proceeded as follows:

- The volume required to store the necessary amount of ammonia, based on the demand for hydrogen to meet energy needs, was calculated.
- An additional 20 % of empty volume was considered as a safety margin.
- The vessel was designed following the methodology outlined by Perry et al. [27] for vertical vessels. Length and diameter were determined based on the total internal volume, with toro-spherical heads considered at the ends.

A critical aspect of storage sizing was the selection of material capable of withstanding ammonia corrosion. Austenitic steel AISI316 was chosen for its suitable properties, as reported in Table 3. These include the tensile strength R_m (MPa) and the yield strength $R_{p,0.2}$ (MPa), fundamental to calculate the thickness necessary to resist the mechanical stress caused by the operating pressure, and the density ρ (kg m^{-3}).

The vessel thickness e (mm) was calculated with the following equation:

$$e = \frac{p \cdot D_i}{2f - P} \tag{2}$$

where p (MPa) is the operative pressure, D_i (mm) is the internal diameter of the tank and $f = \min\left(\frac{R_{p_{0.2}}}{1.5}; \frac{R_m}{2.4}\right)$.

A safety margin of 2.5 mm was added to the calculated thickness to account for corrosion.

Table 3
AISI316 properties.

Parameter	Value	Unit
R_m (20 °C)	515	MPa
$R_{p,0.2}$ (20 °C)	200	MPa
ρ	806	kg m^{-3}

Fig. 1. Block diagram of the main sections of the storage system.

After calculating the thickness of the tank, it was possible to proceed with the calculation of the volume of the empty vessel.

The total weight of the storage system comprised the sum of the weight of the empty tank and the weight of stored ammonia.

2.2.2. Cracking section

The cracking section encompasses the cracking reactor and upstream equipment required to meet the specified input requirements for the reactor. The cracking reaction occurs at 450 °C and 1 bar in the presence of a ruthenium-based catalyst, within a membrane reactor with hollow fibers. The membrane reactor design, utilizing hollow fibers (HFR), enhances the efficiency of the cracking process by allowing for selective separation of reaction products while maintaining a compact size and optimal conditions within the reactor. This selective permeation helps in maximizing the yield of hydrogen and minimizing the presence of by-products in the downstream [16].

The catalytic process was assumed to be isothermal, leading, at equilibrium, to an ammonia conversion equal to $x_{NH_3} = 99.8\%$.

The reactor was sized starting from literature data of a HFR designed to produce hydrogen for a 100 kW vehicle [16]. The scale-up was performed by maintaining constant the resident time into the reactor τ (s), calculated as function of the reactor volume V_r (m^3) and the volumetric flow rate $\dot{V}_{NH_3}$ (m^3 s^{-1}):

$$\tau = \frac{V_r}{\dot{V}_{NH_3}} \tag{3}$$

The amount of catalyst W_{cat} (kg) was calculated by maintaining the values for bed density ρ_b (kg m^{-3}) and kinetic constant k (s^{-1}) present in the reference paper, using the following formula:

$$W_{cat} = -\rho_b \cdot \frac{\dot{V}_{NH_3}}{k} \cdot \ln(1 - x_{NH_3}) \tag{4}$$

Finally, the scaled-up reactor was sized in terms of weight, intended as the sum of the weight of the structure and the weight of the catalyst.

For the volume scale-up, the area of the square packing $A_{packing}$ (m^2), containing four hollow fibers, was calculated from [16] by considering the total number of hollow fibers ($N_{HF,baseline}$) of the automotive case study:

$$A_{packing} = \frac{4 \cdot A_{HF}}{N_{HF,baseline}} \tag{5}$$

where A_{HF} (m^2) is the area of the single hollow fiber obtained as function of the hollow fiber diameter $D_{packing}$ (m):

$$A_{HF} = \frac{\pi}{4} \cdot \left(\frac{D_{packing}}{2}\right)^2 \tag{6}$$

In this way, the respective number of hollow fibers for the present case study (N_{HF}) was derived.

Assuming a pore diameter D_{pore} of 500 μm, the effective area of the hollow fiber $A_{HF,eff}$ (m^2) was calculated as:

$$A_{HF,eff} = A_{HF} - 4 \cdot \frac{\pi}{4} \cdot D_{pore}^2 \tag{7}$$

Finally, the actual volume $V_{eff,HFR}$ (m^3) and the weight of the system W_{HFR} (kg) were derived:

$$V_{eff,HFR} = 4 \cdot A_{HF,eff} \cdot N_{HF} \cdot L_{HF} \tag{8}$$

$$W_{HFC} = V_{eff,HFC} \cdot (1 - \varepsilon_{HF}) \cdot \rho_{Al_2O_3} + W_{cat} \tag{9}$$

where L_{HF} (m) is the fiber length, $\rho_{Al_2O_3}$ (kg m^{-3}) is the density of the hollow fiber, and ε_{HF} is the porosity of the hollow fiber substrate.

The input parameters used for the calculation are reported in Table 4.

Table 4
Input parameters for reactor scale-up.

Parameter	Value	Unit
x_{NH_3}	0.998	
ρ_b	26	kg m^{-3}
k	2200	h^{-1}
$N_{HF,baseline}$	1100	
D_{pore}	500	μm
L_{HF}	0.85	m
$\rho_{Al_2O_3}$	3940	kg m^{-3}
ε_{HF}	0.43	

2.2.3. Purification section

Following the cracking section, the hydrogen stream underwent a purification step to remove traces of NH$_3$, which are pollutants detrimental to the PEMFC. Adsorption using activated carbon-filled columns was selected for the separation. A specific type of activated carbon impregnated with MgCl$_2$ (4 wt% Mg) was identified in the literature [28], distinguished by its superior adsorption capacity compared to conventional activated carbon.

Since adsorption is an exothermic process, operating at lower temperatures enhances efficiency and reduces the amount of activated carbon needed, leading to weight and equipment volume savings [28]. However, lower temperatures require more cooling in the preceding section, increasing refrigerant demand and necessitating larger, heavier heat exchangers. A sensitivity analysis revealed 40 °C as the trade-off operating temperature for minimizing the size of the equipment while maintaining high adsorption efficiency.

Once the quantity of ammonia mol_{NH_3} (mol) to be removed and the adsorption capacity at 40 °C were determined, the amount of activated carbon $W_{AC,eff}$ (kg) needed per cycle was calculated, assuming 80 % saturation.

$$W_{AC,eff} = \frac{mol_{NH_3}/M_{NH_3}}{0.8} \tag{10}$$

where M_{NH_3} (g mol^{-1}) is the molecular weight of ammonia.

The column volume was computed, considering activated carbon occupies 80 % of total volume and requires replacement every two cycles. Column dimensions, i.e., length L_{ad} (m) and diameter D_{ad} (m) were derived from volume, with an L_{ad}/D_{ad} ratio of 3. Using AISI 316 for column material and estimating thickness as for the storage tank (section 2.2.1), the equipment weight W_{ad} (kg) was estimated as:

$$W_{ad} = W_{emptycolumn} + 2 \cdot W_{AC,eff} \tag{11}$$

where $W_{emptycolumn}$ (kg) represents the weight of the empty column.

Table 5 summarizes the most important features of the equipment.

2.2.4. Hydrogen compression section

Before entering the fuel cell, hydrogen needs to be compressed up to the operating pressure of the fuel cell. The equation for sizing the compressor power P_{compr} (kW) is reported below:

$$P_{compr} = \dot{m} \cdot c_p \cdot T_{in,compr} \cdot \left(\beta^{\frac{\gamma-1}{\gamma}} - 1\right) \cdot \frac{1}{\eta_{is}\eta_{em}} \tag{12}$$

Table 5
Characteristics of the adsorption column.

Parameter	Description	Value	Unit
Mg [28]	Amount of magnesium in the activated carbon	4	%wt
T_{ad}	Operative temperature for adsorption	40	°C
w_{ad}[28]	Adsorption capacity	6.48	mmol$_{NH3}$ g$^{-1}_{AC}$
ρ_{AC}	Density of activated carbon	0.81	g cm^{-3}
L_{ad}/D_{ad}	Length to diameter ratio	3	m m^{-1}

Table 6 shows the most important data relating to the sizing of hydrogen compressor and the relative explaination. In particular, the mass flow rate of hydrogen was calculated with Faraday law considering the fuel cell current i (A), Faraday constant F (C mol^{-1}), the hydrogen molecular weight M_{H_2} (g mol^{-1}) and its stoichiometry ($\lambda_{H_2} = 1$).

2.3. Fuel cell section

FC system is constituted by the fuel cell stacks, the air compressor, the cooling system, and other auxiliaries (valves, pumps…). The following paragraph describes the calculation of the weights of the main equipment of this system. For more details, the sizing procedure employed for the fuel cell system was partially derived from our previous work [29].

2.3.1. Compression section

While the power required for hydrogen compression remains consistent across various mission profiles, dictated solely by storage and release conditions, additional considerations must be made for the air compressor. In fact, the reactant air is sourced from the external environment, where temperature and pressure conditions vary depending on the altitude of the mission profile. The sizing of this equipment was conducted by selecting the cruise condition as the designing point, corresponding to the lowest external pressure and thus resulting in the maximum compression ratio. The external air conditions were calculated with equations detailed in [29].

A two-stage compressor was selected due to the high compression ratio required and commercial models were used to derive the gravimetric and volumetric indexes, equal to 1.03 kW kg^{-1} and 1.05 kW L^{-1}, respectively [30].

Table 7 shows the most important data relating to the sizing of air compressor. In particular, the mass flow rate was calculated with Faraday law as for hydrogen, considering the air stoichiometry λ_{air} of 1.75 and oxygen volumetric concentration in air y_{O_2}.

2.3.2. Fuel cell stack

For the sizing of the fuel cell stack, differently from ref. [29], a commercial model was considered to estimate its weight and occupied volume. PowerCellution manufactured by PowerCell [31] was selected for this purpose, with the features detailed in Table 8.

Once the polarization curve of the commercial fuel cell stack was defined, the operating point was determined as the nominal one because of the higher electrochemical efficiency. The sizing of the fuel cell involved calculating the number of stacks (N_{stack}) required to meet the electrical demands of both auxiliary components and the aircraft propulsion system at every point of the mission profile. According to our previous studies [4,29], the take-off stage was identified as the mission phase requiring the highest amount of gross power from the fuel cell, and this point was used as the design reference.

2.3.3. Thermal management system

The thermal management system (TMS) comprises two subsystems: the high thermal cooling (HTC) and the low thermal cooling (LTC) systems. The HTC is responsible for cooling the fuel cell, ensuring that

Table 6
Input parameters for sizing hydrogen compressor.

Parameter	Description	Value	Unit
$\dot{m}$	Inlet flow rate	$\lambda_{H_2} \cdot \dfrac{i}{2F} M_{H_2}$	
c_p	Specific heat capacity	14.3	kJ kg^{-1} K^{-1}
$T_{in,compr}$	Inlet temperature	40	°C
β	Compression ratio	2	
γ	Polytropic exponent	1.41	
η_{is}	Isentropic efficiency	0.78	
η_{em}	Electro-mechanic efficiency	0.90	

Table 7
Input parameters for sizing air compressor.

Parameter	Description	Value	Unit
$\dot{m}$	Inlet flow rate	$\dfrac{\lambda_{air}}{y_{O_2}} \cdot \dfrac{i}{4F} M_{air}$	
c_p	Specific heat capacity	1.005	kJ kg^{-1} K^{-1}
$T_{in,compr}$	Inlet temperature	function of h	°C
β	Compression ratio	function of h	
γ	Polytropic exponent	1.4	
η_{is}	Isentropic efficiency	0.80	
η_{em}	Electro-mechanic efficiency	0.88	
h	Altitude	25,000	ft

Table 8
Main features of PowerCellution 125 kW [31].

Stack configuration		
Max power output	125	kW
Cell count	455	
Dimensions	420x582x156	mm
Weight	42	kg
Performance		
Operating temperature	80	°C
Operating pressure	2	bar

the heat produced during the electrochemical reaction is efficiently removed to maintain the fuel cell's temperature within its operating range; the LTC handles the cooling of the air which, after compression, could be at a higher temperature than the required operating one.

For the HTC, a refrigerant fluid was sent to the cooling plates of the fuel cell to remove the produced heat, and its temperature was brought back to the initial one in a closed circuit with an air radiator. In this high-temperature circuit, GLYSANTIN® 50/50 v/v% was selected as refrigerant [32], working between 60 °C ($T_{in,coolant}$) and 90 °C ($T_{out,coolant}$). Usually, the cooling system is sized so that the temperature variation of the refrigerant fluid is equal to 10 °C. However, an optimized thermal management architecture for PEMFC was found in the literature [33], in which the FC system is divided into several units in series from the point of view of the flow of the refrigerant fluid. In this way, each FC unit operates at different temperatures, but each unit has a driving force of 10 °C, while the driving force of the whole system will be higher. This method allows not only to reduce the flow rate of refrigerant fluid (and therefore the quantity to be stored on the aircraft) but also allows a reduction of the exchange area and the weight of the radiator.

It was decided to carry out the calculation using this method and dividing the FC system into three units: in this way the refrigerant fluid has a global temperature increment of 30 °C, generating a considerable saving in terms of weight.

The first step in the sizing procedure was the definition of heat to be removed from the fuel cell Q_{HTC} (kW), calculated as follows, assuming 10 % of the heat was already dissipated by convective fluxes of reactants in the cell:

$$Q_{HTC} = N_{cell} \bullet N_{stack} \bullet i \bullet (E_{th} - E_{cell}) \bullet (1 - 0.10) \qquad (13)$$

where N_{cell} is the number of cells in a single stack, N_{stack} is the total number of the stacks, i (A) is the operative current of the PEMFC, E_{th} (V) and E_{cell} (V) represent the theoretical and the operative potentials, respectively.

For the sizing of the radiator, the calculation was carried out in the take-off phase, considering the worst external conditions of 40 °C for the inlet of air in the radiator ($T_{in,air}$), and imposing a driving force of 15 °C. The sizing procedure was detailed elsewhere [29].

The volume and the weight of the radiator were defined with indexes derived from literature, intended as surface gravimetric density and surface volumetric density [34].

The total weight of the equipment was given by the sum of the heat exchanger, auxiliaries (pump, fan) and refrigerant fluid to be loaded in the closed circuit. The weight of the auxiliaries was estimated as 10 % of the overall cooling system weight.

For the LTC system, the sizing procedure was almost the same, calculating the heat to be removed Q_{LTC} (kW) as:

$$Q_{LTC} = \dot{m}_{coolant} \cdot c_{p,coolant} \cdot \left(T_{out,LTC} - T_{in,LTC} \right) \tag{14}$$

where $\dot{m}_{coolant}$ (kg s^{-1}) is the coolant flow rate, $c_{p,coolant}$ (kJ kg^{-1} K^{-1}) is its specific heat capacity, $T_{out,LTC}$ (°C) and $T_{in,LTC}$ (°C) represent the system outlet and inlet temperature, respectively.

The parameters used for sizing the cooling system are reported in Table 9.

2.4. Thermal integration

The thermal integration is crucial within the electrified propulsion system, as there are several thermal management systems to handle in addition to those described for the fuel cell and the compressor. Specifically:

- The ammonia stream needs to be heated from ambient temperature to 450 °C before entering the reactor due to the cracking operating temperature;
- The hydrogen stream exiting the reactor must be cooled down to 40 °C to efficiently undergo the exothermic adsorption process.
- The hydrogen stream exiting the compressor must be cooled down to 80 °C before entering the fuel cell.

So, there is a heating section and a cooling section that could potentially be integrated to minimize heat exchangers and dedicated fluids.

The heating section was designed with two heat exchangers in which the ammonia is pre-heated by energy integration with the reaction products and with the hydrogen exiting the compressor, respectively. Additionally, a furnace was designed to heat ammonia completely up to the operating temperature of the reactor.

The cooling section was designed to bring the temperature of the hydrogen stream down to 40 °C before entering the purification section. GLYSANTIN® was selected as coolant, in alignment with the PEMFC cooling system, with temperature variations ranging between 10 °C and 30 °C. The described cooling section comprises a closed circuit with two equipment: the first is a heat exchanger where the hydrogen stream is cooled using the refrigerant fluid, and the second is a radiator where the refrigerant is cooled back to its initial temperature using air.

The sizing of the heat exchangers was carried out following the trial-and-error procedure proposed by Kern [35] for shell and tube counter-current heat exchangers, while the radiator was sized as described in paragraph 2.3.3.

The constraints of the first pre-heating exchanger were the hydrogen inlet and outlet temperature. For the second pre-heating exchanger, the constraint was instead the temperature of the outgoing ammonia stream, which must be heated up to 380 °C.

Once the calculation procedure and the verification of the U exchange factor was performed, the number of pipes, the diameter of the shell and the length of the exchanger were obtained. The material selected for the design of the exchangers was AISI 316, as one of the treated streams is pure ammonia.

The calculation of the weight of each exchanger was carried out by adding the weights of shell, pipes and end plates. Before calculating the weight, however, the thickness of the various components must be known. For the shell the procedure is the same as for the ammonia storage system; for the pipes, the thickness was defined in the design phase; for the plate the thickness was estimated as 15 times the thickness of the shell.

As far as the furnace is concerned, given the difficulty of finding sizing methods in the literature due to the low flow rates involved, it was decided to derive the size from commercial models manufactured by York [36]. Ammonia enters the furnace at 380 °C and must be heated to the reaction temperature of 450 °C. As fuel it was necessary to decide whether to still use ammonia, or a part of the hydrogen produced by cracking. Hydrogen is characterized by a very high calorific value, but it is still necessary to store a greater quantity of ammonia to produce both the hydrogen to be sent to the fuel cells system and that to be burned in the furnace. To choose the fuel it is therefore necessary to calculate in which of the two cases the quantity of excess ammonia to be stored is less.

Table 10 and Table 11 report the most important characteristics of the heating and cooling section and of the furnace, respectively.

Table 9
Set parameters for the sizing of both HTC and LTC systems [29].

HTC system			
$T_{in,coolant}$	60	°C	Inlet temperature of FC coolant
$T_{out,coolant}$	90	°C	Outlet temperature of FC coolant
U	0.1	kJ kg^{-1} K^{-1}	Global heat coefficient
LTC system			
$T_{in,LTC}$	190	°C	Inlet temperature of air (equal to air temperature at compressor outlet)
$T_{out,LTC}$	80	°C	Outlet temperature of air (equal to FC operative temperature)
U	0.1	kJ kg^{-1} K^{-1}	Global heat coefficient
General parameters			
$c_{p,coolant}$	3.55	kJ kg^{-1} K^{-1}	Specific heat capacity of coolant
$c_{p,air}$	1.005	kJ kg^{-1} K^{-1}	Specific heat capacity of air
$t_{coolant}$	10	s	Circulation time of liquid coolant into the circuit
$T_{in,air}$	40	°C	Inlet temperature of air in the radiator
$T_{out,air}$	55	°C	Outlet temperature of air from the radiator
ε	0.7		Effectiveness
Grav. surface density	1.0	kg m^{-2}	Gravimetric surface density
Vol. surface density	800	m^2 m^{-3}	Volumetric surface density

Table 10
Input parameters for the heating section.

Heating section			
		Pre-heating 1	**Pre-heating 2**
Cold fluid	Type of fluid	Ammonia from storage	Ammonia from Pre-heating 1
	T inlet	25 °C	*Defined by Pre-heating 1*
	T outlet	Calculated	380 °C
Hot fluid	Type of fluid	Hydrogen from purification	Hydrogen from reactor
	T inlet	*Defined by compression*	450 °C
	T outlet	80 °C	*Calculated*
Cooling section			
		Cooling 1	**Radiator**
Cold fluid	Type of fluid	Glysantin	Air
	T inlet	10 °C	40 °C
	T outlet	30 °C	55 °C
Hot fluid	Type of fluid	Hydrogen from pre-heating 2	Glysantin
	T inlet	*Defined by pre-heating 2*	30 °C
	T outlet	40 °C	10 °C

Table 11
Furnace parameters.

Parameter	Value	Unit
T inlet	380	°C
T outlet	450	°C
LHV Ammonia	18.6	MJ kg^{-1}
LHV Hydrogen	120	MJ kg^{-1}

Table 12
Characteristics of ammonia tank.

Input parameters		
H$_2$ to produce	365	kg
NH$_3$ required	2057	kg
Storage tank		
Volume	4.0	m^3
Length	3.0	m
Diameter	1.3	m
Thickness	7.5	mm
Weight	84.5	kg

3. Results and discussion

The identified architecture of the storage system is depicted in Fig. 2.

The energy integration between pure ammonia, sourced from the 25 °C tank and requiring heating for entry into the reactor, and the hydrogen stream, which necessitates heating to meet the fuel cell system's inlet temperature, is observable. This integration is facilitated by the heat exchanger labelled "pre-heating 1″ in the figure. Subsequently, the ammonia flow undergoes additional heating through the "pre-heating 2″ heat exchanger. This is accomplished by transferring heat
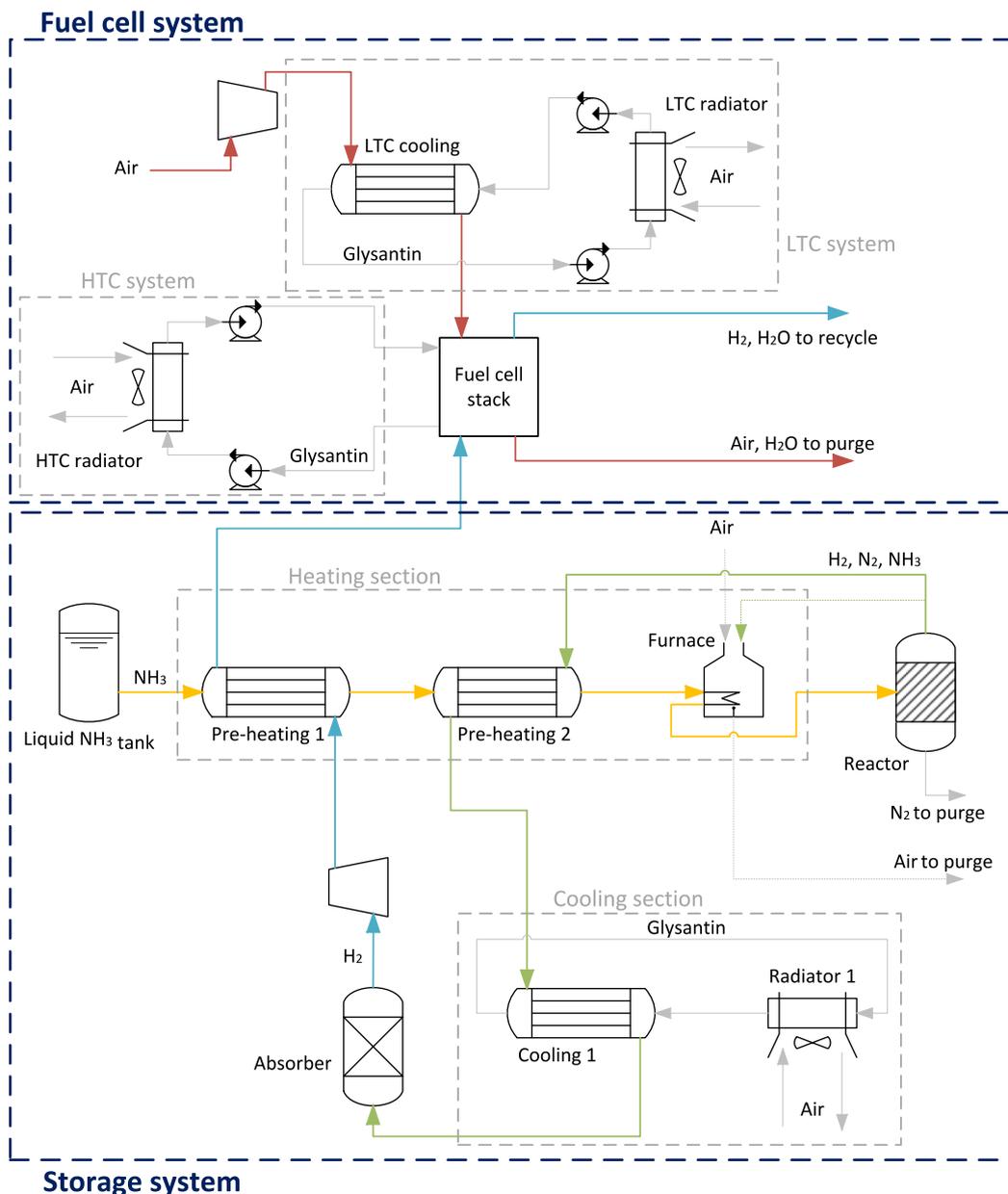
from the H$_2$/NH$_3$ stream exiting the reactor, which, in turn, must be cooled before entering the purification process.

3.1. Storage system

The storage system outlined in this case study, as detailed in the

Fig. 2. Block flow diagram representing the hydrogen storage system thermally integrated with the PEM fuel cell system.

Table 13

Sizing of components for the thermal management of hydrogen storage system.

Heating section			
		Pre-heating 1	**Pre-heating 2**
Cold fluid	Type of fluid	Ammonia from storage	Ammonia from Pre-heating 1
	T inlet	25 °C	101 °C
	T outlet	101 °C	380 °C
Hot fluid	Type of fluid	Hydrogen from purification	Hydrogen from reactor
	T inlet	143 °C	450 °C
	T outlet	80 °C	208 °C
Sizing	Heat	45.5 kW	179.5 kW
	Number of tubes	109	203
	Tube diameter	18.3 mm	18.3 mm
	Shell diameter	0.34 *m*	0.45 *m*
	Shell thickness	3.5 mm	3.5 mm
	Length	1.83 *m*	2.44 *m*
	Volume	0.17 m^3	0.38 m^3
	Weight	27.5 kg	53.6 kg

Cooling section			
		Cooling 1	**Radiator**
Cold fluid	Type of fluid	Glysantin	Air
	T inlet	10 °C	40 °C
	T outlet	30 °C	55 °C
Hot fluid	Type of fluid	Hydrogen from pre-heating 2	Glysantin
	T inlet	208 °C	30 °C
	T outlet	40 °C	10 °C
Sizing	Heat	122.2 kW	124.4 kW
	U	–	0.1 kW m^{-2} K^{-1}
	E	–	0.5
	Number of tubes	61	–
	Tube diameter	18.3 mm	–
	Shell diameter	0.26 m	–
	Shell thickness	3.5 mm	–
	Length	1.83 m	–
	Volume	0.1 m^3	0.1 m^3
	Weight	21.5 kg	82.9 kg

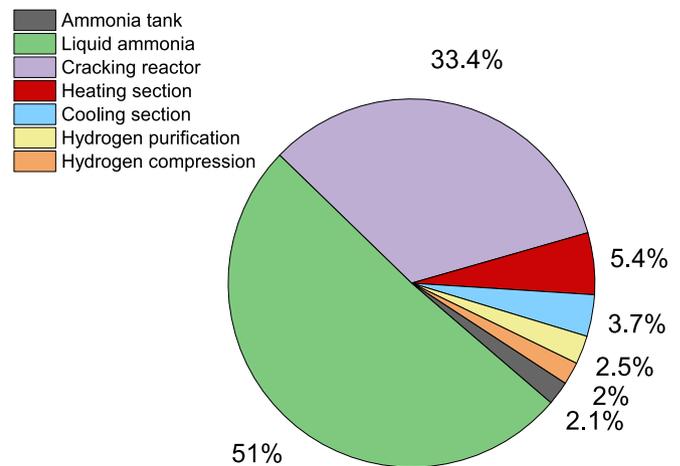**Fig. 3.** Weight distribution of hydrogen storage system.

methodology section, comprises several key components: the ammonia tank, the reactor, the absorber, and the heat exchangers for managing the flow of hydrogen and ammonia throughout the storage system.

To meet the power demands for a two-hour flight, 365 kg of hydrogen is required, calculated based on the fuel cell efficiency. This translates to 2057 kg of ammonia, which was the input parameter for calculating the size of ammonia tank, with its specific characteristics reported in Table 12.

The hollow fiber converter was designed to maintain a consistent residence time into the reactor, aligning with literature data indicating a value of 0.86 s. This duration ensures an ammonia conversion of 99.8 %, as reported in literature. This design resulted in a total volume of 0.7 m^3, accommodating 4243 packing units of hollow fibers.

Furthermore, the total weight of the hollow fiber reactor, including both its structural elements and catalyst, amounts to 1347 kg.

The third fundamental step in hydrogen release involves the absorption of the product stream from the cracking reactor to eliminate any remaining traces of ammonia. Sufficient activated carbon was allocated to purify hydrogen for two flights, totaling 93.2 kg. Based on this requirement, a size of 0.14 m^3 was determined, with dimensions of 1.18 m in length and 0.39 m in diameter. Consequently, the total weight amounted to 101.1 kg.

The thermal management segment was appropriately dimensioned with the findings detailed in Table 13 for the integrated section and Table 14 for the furnace. Specifically, the utilization of hydrogen as a fuel in the furnace resulted in a minimal increase in its storage weight, amounting to just 1.1 %, due to its higher heating value compared to ammonia. The commercial furnace selected for this purpose was the GAS FURNACE X-13 MOTOR with a capacity of 100,000 BTU (29.3 kW), so two furnaces in series were allocated.

Finally, the last component of the storage system was the hydrogen compressor, which size was estimated equal to 80 kg.

The sizing procedure results in a total weight of the storage system equal to 4036 kg, with a gravimetric index of 9.1 %, representing the mass of hydrogen stored relative to the overall weight of the storage system. Fig. 3 illustrates the distribution of weights among the various components of the system. It is evident that the primary contributors to the overall weight are the ammonia itself (51 %) and the cracking reactor (33 %). Conversely, the secondary equipment responsible for adjusting the streams to meet the operational conditions of different sections (such as heating, cooling, compression, and purification) does not significantly affect the system's weight. Collectively, their impact on the entire system weight is approximately 16 %.

Table 14

Sizing of furnace for pre-heating of ammonia up to the reactor operating temperature.

Parameter	Value	Unit
Total heat to provide	56	kW
Furnace model	X-13 MOTOR 100000 BTU 2000CFM 95 %, TM9E100C20MP12-C	
Combustion efficiency	0.95	
Single furnace capacity	29.3	kW
Number of furnaces	2	
Weight of fuel required	21.6	kg
NH$_3$ increase	1.1	%
Volume	0.87	m^3
Weight	138	kg

3.2. Fuel cell system

In sizing the fuel cell system, the power contribution from each component was preliminarily calculated in its design point.

Then, the total electrical power required was defined, encompassing the propulsion power during take-off (designated as the point with maximum gross power requirement in the mission profile) and the power demands from auxiliary components (such as compressors, pumps, valves, etc.). The obtained value of gross electrical power facilitated the determination of the number of commercial stacks and, subsequently, the final dimensions of the electrochemical stack rack.

The results in terms of electrical power, weights and volumes for each component of the fuel cell system are reported in Table 15, while their weight distribution is depicted in Fig. 4.

As expected, half of the weight of the fuel cell system is attributed to the thermal management of the fuel cell. However, the optimized thermal management technique outlined in the methodology (paragraph 2.3.3), which employs the step-fractioned driving force, led to a weight saving of approximately 27 % compared to the conventional system. In the conventional setup, the lower driving force necessitated a larger radiator, contributing to this difference.

Based on the results obtained, the specific power of the fuel cell system was estimated at 0.7 kW/kg, consistent with the current data found in literature.

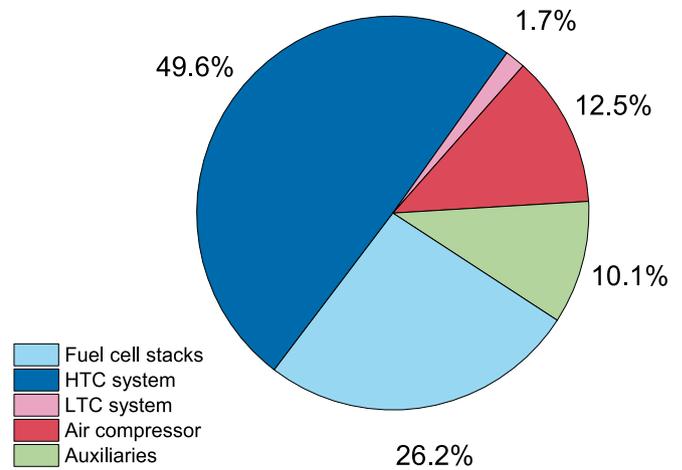## 3.3. Comparison with conventional propulsion system

In the previous paragraphs, the design of both the storage and fuel cell systems was presented. Subsequently, the overall weight of the designed electrified propulsion system, comprising the storage system, fuel cell system and electric motor, was compared with the conventional kerosene-based propulsion system of the ATR 72–600. The comparison revealed that retrofitting the aircraft with the installation of the innovative system incurred a weight increase of 26 %. Consequently, addressing this weight increment necessitates strategies such as augmenting the required take-off power, potentially oversizing the propulsion system, or reducing the payload by up to 80 %.

To make the ammonia-based system feasible with current technologies, innovative architectures must be devised to counterbalance the aircraft's weight increment. Moreover, optimization efforts should focus on components with the most significant impact on overall weight, including the thermal management system of the fuel cell, the ammonia storage and the subsequent hydrogen release system, as depicted in Fig. 5. An indirect method to optimize the system would involve enhancing the efficiency of the fuel cell. This improvement would
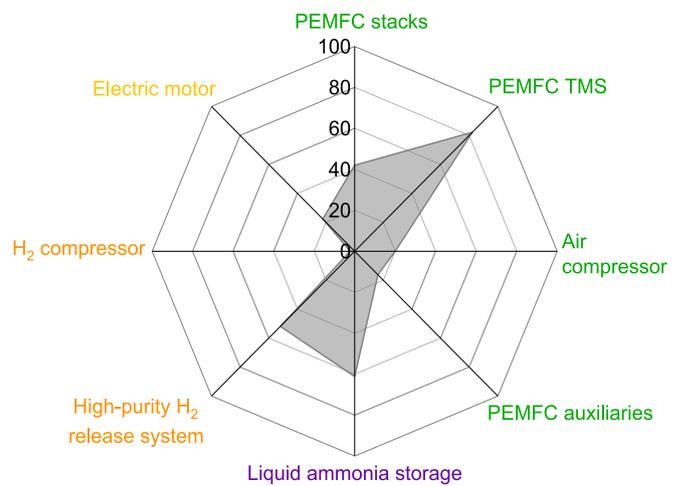

Fig. 4. FC system weight distribution.

Fig. 5. Percentage impact of the different sections of the electrified propulsion system on its overall weight.

benefit both the thermal management system and the required quantities of reactants. Additionally, optimizing the operational conditions, such as pressure and temperature, would further enhance system efficiency.

4. Conclusions

This study demonstrates the feasibility of using ammonia as a hydrogen storage medium for a fully electrified propulsion system based on PEMFCs. A preliminary analysis yields a gravimetric hydrogen storage index of 9.1 %, which positions ammonia as a competitive solution for hydrogen storage. Moreover, the use of ammonia instead of pure hydrogen enhances onboard safety due to milder storage conditions and offers a cost-effective solution for hydrogen transportation and storage.

A systemic approach was employed to assess the potential of this storage method coupled with PEMFC system for regional aviation. While the system is theoretically viable, it currently faces a challenge in competitiveness, with an estimated 26 % increase in the MTOW compared to conventional kerosene-based systems. This increase would likely require reducing the payload to maintain the MTOW weight or optimizing the aircraft's architecture to reduce structural weight, thus allowing for more weight allocation to storage. The main contributors to the size of the proposed system are the amount of liquid ammonia to store, together with the fuel cell thermal management system.

Improving fuel cell efficiency, as well as optimizing system

Table 15
Sizing results for each component of the fuel cell system.

Parameter		Value	Unit
Mass of H_2		365	kg
Fuel cell	Number of stacks	35	
	Nominal power tot (gross)	4114	kW
	Nominal power tot (net)	3691	kW
	Mass of FC stacks	1470	kg
	Volume of FC stacks	1.33	m^3
Compressor	Sizing power	820	kW
	Weight	702	kg
	Volume	0.69	m^3
HTC system	Sizing power	3045	kW
	Weight	2784	kg
	Volume	2.8	m^3
LTC system	Sizing power	412	kW
	Weight	94	kg
	Volume	0.11	m^3
Auxiliaries (valves, pumps…)		568	kg

integration, is critical to improving performance and reducing overall weight. Additionally, the optimization of the operating conditions and the equipment integration can increase the specific power of the overall propulsive system in terms of kW/kg and kW/L. Further research is essential to optimize energy efficiency, such as by exploring direct-ammonia fuel cell options (e.g., HT-PEMFC), which could enhance thermal integration and reduce system weight.

With this approach, the potential of ammonia as a hydrogen carrier for aviation has been clearly defined, along with the critical technological gaps that must be addressed. Key areas for optimization have been identified to enable its practical implementation. Ultimately, this work emphasizes ammonia's role in advancing sustainable aviation and sets the foundation for the transition to greener, electrified propulsion systems.

CRediT authorship contribution statement

Maria Chiara Massaro: Writing – review & editing, Writing – original draft, Investigation, Formal analysis, Data curation, Conceptualization. **Federico Aluia:** Methodology, Formal analysis, Data curation. **Roberta Biga:** Writing – review & editing, Supervision, Formal analysis. **Grazia Accardo:** Writing – review & editing. **Alessandro Hugo Antonio Monteverde:** Writing – review & editing, Supervision, Resources, Conceptualization.

Declaration of competing interest

The authors declare that they have no known competing financial interests or personal relationships that could have appeared to influence the work reported in this paper.

Acknowledgements

Data availability

Data will be made available on request.

References

[1] Reducing emissions from aviation. European Commission Website n.d. https://climate.ec.europa.eu/eu-action/transport/reducing-emissions-aviation_en (accessed August 31, 2023).

[2] Schäfer AW, Barrett SRH, Doyme K, Dray LM, Gnadt AR, Self R, et al. Technological, economic and environmental prospects of all-electric aircraft. Nat Energy 2019;4:160–6. https://doi.org/10.1038/s41560-018-0294-x.

[3] McKinsey & Company. Hydrogen-powered aviation – A fact-based study of hydrogen technology, economics, and climate impact by 2050. 2020. Doi: https://data.europa.eu/doi/10.2843/471510.

[4] Massaro MC, Biga R, Kolisnichenko A, Marocco P, Monteverde AHA, Santarelli M. Potential and technical challenges of on-board hydrogen storage technologies coupled with fuel cell systems for aircraft electrification. J Power Sources 2023; 555. https://doi.org/10.1016/j.jpowsour.2022.232397.

[5] Cechetto V, Di Felice L, Medrano JA, Makhloufi C, Zuniga J, Gallucci F. H2 production via ammonia decomposition in a catalytic membrane reactor. Fuel Process Technol 2021;216. https://doi.org/10.1016/j.fuproc.2021.106772.

[6] - International Energy Agency I. Global Hydrogen Review 2022. 2022.

[7] Stolz B, Held M, Georges G, Boulouchos K. Techno-economic analysis of renewable fuels for ships carrying bulk cargo in Europe. Nat Energy 2022;7:203–12. https://doi.org/10.1038/s41560-021-00957-9.

[8] ADVANCED RESEARCH PROJECTS AGENCY – ENERGY (ARPA-E) U.S. DEPARTMENT OF ENERGY. RENEWABLE ENERGY TO FUELS THROUGH UTILIZATION OF ENERGY-DENSE LIQUIDS (REFUEL) n.d.

[9] Boretti A, Castelletto S. NH3Prospects in Combustion Engines and Fuel Cells for Commercial Aviation by 2030. ACS Energy Lett 2022;7:2557–64. https://doi.org/10.1021/acsenergylett.2c00994.

[10] Yu Y, Luo C, Min H, Cao Q, Jiang J, Wu H. Role of proton exchange membrane fuel cell in efficiency improvement of ammonia–hydrogen fusion zero-carbon powertrains for long-haul, heavy-duty transportation. Energy Convers Manag 2024;309. https://doi.org/10.1016/j.enconman.2024.118425.

[11] Makhloufi C, Kezibri N. Large-scale decomposition of green ammonia for pure hydrogen production. Int J Hydrogen Energy 2021;46:34777–87. https://doi.org/10.1016/j.ijhydene.2021.07.188.

[12] Lucentini I, Garcia X, Vendrell X, Llorca J. Review of the Decomposition of Ammonia to Generate Hydrogen. Ind Eng Chem Res 2021;60:18560–611. https://doi.org/10.1021/acs.iecr.1c00843.

[13] pidjoe. The Future of Hydrogen. n.d.

[14] Park Y, Cha J, Oh HT, Lee T, Lee SH, Park MG, et al. A catalytic composite membrane reactor system for hydrogen production from ammonia using steam as a sweep gas. J Memb Sci 2020;614. https://doi.org/10.1016/j.memsci.2020.118483.

[15] Cerrillo JL, Morlanés N, Kulkarni SR, Realpe N, Ramírez A, Katikaneni SP, et al. High purity, self-sustained, pressurized hydrogen production from ammonia in a catalytic membrane reactor. Chem Eng J 2022;431. https://doi.org/10.1016/j.cej.2021.134310.

[16] Mazzone S, Campbell A, Zhang G, García-García FR. Ammonia cracking hollow fibre converter for on-board hydrogen production. Int J Hydrogen Energy 2021;46: 37697–704. https://doi.org/10.1016/j.ijhydene.2021.09.038.

[17] Engelbrecht N, Chiuta S, Bessarabov DG. A highly efficient autothermal microchannel reactor for ammonia decomposition: Analysis of hydrogen production in transient and steady-state regimes. J Power Sources 2018;386: 47–55. https://doi.org/10.1016/j.jpowsour.2018.03.043.

[18] Cha J, Jo YS, Jeong H, Han J, Nam SW, Song KH, et al. Ammonia as an efficient COX-free hydrogen carrier: Fundamentals and feasibility analyses for fuel cell applications. Appl Energy 2018;224:194–204. https://doi.org/10.1016/j.apenergy.2018.04.100.

[19] Comotti M, Frigo S. Hydrogen generation system for ammonia-hydrogen fuelled internal combustion engines. Int J Hydrogen Energy 2015;40:10673–86. https://doi.org/10.1016/j.ijhydene.2015.06.080.

[20] Ezzat MF, Dincer I. Comparative assessments of two integrated systems with/without fuel cells utilizing liquefied ammonia as a fuel for vehicular applications. Int J Hydrogen Energy 2018;43:4597–608. https://doi.org/10.1016/j.ijhydene.2017.07.203.

[21] Al-Hamed KHM, Dincer I. A novel ammonia solid oxide fuel cell-based powering system with on-board hydrogen production for clean locomotives. Energy 2021; 220. https://doi.org/10.1016/j.energy.2021.119771.

[22] Di Legge G, Nabavi SA, Mazzei L, Da Soghe R, Bianchini C, Amiri A, et al. Ammonia powered solid oxide fuel cells for general aviation propulsion systems: challenges and opportunities. Computer Aided Chemical Engineering, vol. 52, Elsevier B.V.; 2023, p. 2351–61. Doi: 10.1016/B978-0-443-15274-0.50374-7.

[23] Ye M, Sharp P, Brandon N, Kucernak A. System-level comparison of ammonia, compressed and liquid hydrogen as fuels for polymer electrolyte fuel cell powered shipping. Int J Hydrogen Energy 2022;47:8565–84. https://doi.org/10.1016/j.ijhydene.2021.12.164.

[24] Lin L, Zhang L, Luo Y, Luo J, Chen C, Jiang L. Highly-integrated and Cost-efficient Ammonia-fueled fuel cell system for efficient power generation: A comprehensive system optimization and Techno-Economic analysis. Energy Convers Manag 2022; 251. https://doi.org/10.1016/j.enconman.2021.114917.

[25] Hunter HMA, Makepeace JW, Wood TJ, Mylius OS, Kibble MG, Nutter JB, et al. Demonstrating hydrogen production from ammonia using lithium imide – Powering a small proton exchange membrane fuel cell. J Power Sources 2016;329: 138–47. https://doi.org/10.1016/j.jpowsour.2016.08.004.

[26] Cinti G, Liso V, Sahlin SL, Araya SS. System design and modeling of a high temperature PEM fuel cell operated with ammonia as a fuel. Energies (basel) 2020; 13. https://doi.org/10.3390/en13184689.

[27] Perry RH. Perry's chemical engineers' handbook. 6th ed. New York: 1984.

[28] Hong MW, Park JH, Win MZ, Yoon HC, Yi KB. Enhanced ammonia adsorption performance of MgCl2-loaded activated carbon in pressure swing adsorption. J Ind Eng Chem 2023;118:216–25. https://doi.org/10.1016/j.jiec.2022.11.007.

[29] Massaro MC, Pramotton S, Marocco P, Monteverde AHA, Santarelli M. Optimal design of a hydrogen-powered fuel cell system for aircraft applications. Energy Convers Manag 2024;306:118266. https://doi.org/10.1016/j.enconman.2024.118266.

[30] Rotrex Website. EK40 fuel cell compressor n.d. https://rotrex-fuel-cell-compressor.com/fuel-cell-compressors/ (accessed November 23, 2023).

[31] PowerCell Cellution. datasheet. n.d.

[32] GLYSANTIN® FC G20® ELECTRIFIED Brochure n.d. https://www.glysantin.com/global/en.html (accessed November 23, 2023).

[33] Link A, Ludowicy J, Staggat M. ASSESSMENT OF A SERIAL COOLING CONCEPT FOR HTPEM FUEL CELL SYSTEMS FOR AVIATION APPLICATIONS. n.d.

[34] Schmelcher M, Häßy MarcSchmelcher J. Hydrogen fuel cells for aviation? A potential analysis comparing different thrust categories. ISABE 2022.

[35] Kern DQ. Process Heat Transfer. N Y 1950.

[36] York International Corporation. Technical Guide: YORK® Sun™ Choice AV15 to AV28 2019. https://www.york.com/ (accessed July 31, 2024).